Chemical Engineering Journal 165 (2010) 720–727

Contents lists available at ScienceDirect

Chemical Engineering Journal

journal homepage: www.elsevier.com/locate/cej

Self-catalytic growth and characterization of composite (GaN, InN) nanowires

Hyoun Woo Kim*, Hyo Sung Kim, Han Gil Na, Ju Chan Yang, Sang Sub Kim, Chongmu Lee

Division of Materials Science and Engineering, Inha University, 253 Yong Hyun Dong, Nam Gu, Incheon 402-751, Republic of Korea

ARTICLE INFO

Article history:
Received 2 July 2010
Received in revised form
11 September 2010
Accepted 24 September 2010

Keywords:
Gallium nitride
Indium nitride
Nanowires

ABSTRACT

Composite nanowires consisting of GaN and InN phases were synthesized by heating a mixture of GaN and In powders. The tip nanoparticles also contained GaN and InN phases, in which the InN phases were favored at a lower growth temperature of 600 °C. The associated growth mechanisms are believed to involve a self-catalytic vapor–solid–liquid process, in which the composite nanoparticles located at the tips of the nanowires served as a catalyst. Both the Raman and photoluminescence spectra showed GaN- and InN-related peaks, which agrees with the X-ray diffraction and transmission electron microscopy data.

© 2010 Elsevier B.V. All rights reserved.

1. Introduction

III–V compound nanowires and related quasi one-dimensional (1D) nanostructures have attracted considerable attention owing to their innovative physical and chemical properties and potential applications to electronic and photonic nanoscale devices [1–5]. As a wide band gap (3.4 eV at room temperature) semiconductor, gallium nitride (GaN) 1D nanostructures are the focus of current research because of their promise for use as high-speed field effect transistors, high-temperature electronic devices, UV or blue light emitters, detectors and gas sensors [6–9]. On the other hand, indium nitride (InN) is an important member of group III-nitrides with the lowest electron effective mass [9] and small band gap [10] among all III-nitride semiconductors, suggesting that it can be used in light emitting devices and high speed electronic devices. In particular, by controlling the indium composition, In_xN_y-related compounds, including $In_xGa_{1-x}N$ and $In_xAl_{1-x}N$, have been used for band-gap engineering, which have extended the emission of nitride-based light-emitting diodes (LEDs) from the ultraviolet to near infrared region [11]. InN-based field effect transistors (FETs) have extremely high speeds with a cutoff frequency > 1 THz for 0.1 μm gates [12]. In addition, InN can be used in tandem solar cells [13] and thermophotovoltaic systems [14].

With the individual materials exhibiting the excellent properties, GaN/InN composites can provide suitable properties for use as components in future nanodevices and systems. Due to the large difference between the band gaps of GaN and InN, a conduction-band offset between these two materials should be large enough, enabling the in situ fabrication of GaN Schottky diodes by InN contact [15,16]. Moreover, the development of nanotechnology has led to the fabrication of lattice-mismatched InN/GaN heterostructure nanowires [17].

In this study, a mixture of In and GaN powders was heated and novel composite nanowires were fabricated based on GaN and InN phases. In addition, the composition of nanoparticles corresponded to a mixture of GaN and InN. The mixture-tipped nanowires produced in the present work can be utilized as a mixture or as an individual functional material with porosity if one component is removed selectively. GaN nanowires have been emerged as a promising nanomaterial for oproelectronic devices, such as light-emitting diodes, due to its blue-emitting luminescence. Combining InN to GaN will facilitate the red-shift of the overall PL emission. By controlling the ratio of InN/GaN phases, we will change the emission properties, contributing to the fabrication of more useful optoelectronic devices.

The components in the final product originate partially from vapor precursors (N) and partially from the 'catalyst' itself (Ga and In). Therefore, this study employed extended VLS mechanisms, which provide a new possibility for exploring some novel compound nanowires or nanotubes. The use of the present technology not only extends the conventional VLS mechanism to a broad range of catalytic processes but also provides a new route for the growth of nanocomposites for commercial production. There have been numerous papers on the GaN nanowires or InN nanowires. However, there has been no report on the fabrication of nanowires which are comprised of composites of GaN and InN. Furthermore, to the best of our knowledge, composite nanowires consisting of randomly positioned two different crystalline phases have never been reported. In addition, the ratio of GaN and InN phases in the

* Corresponding author. Tel.: +82 10 8428 0883.
E-mail address: hwkim@inha.ac.kr (H.W. Kim).

1385-8947/$ – see front matter © 2010 Elsevier B.V. All rights reserved.
doi:10.1016/j.cej.2010.09.035

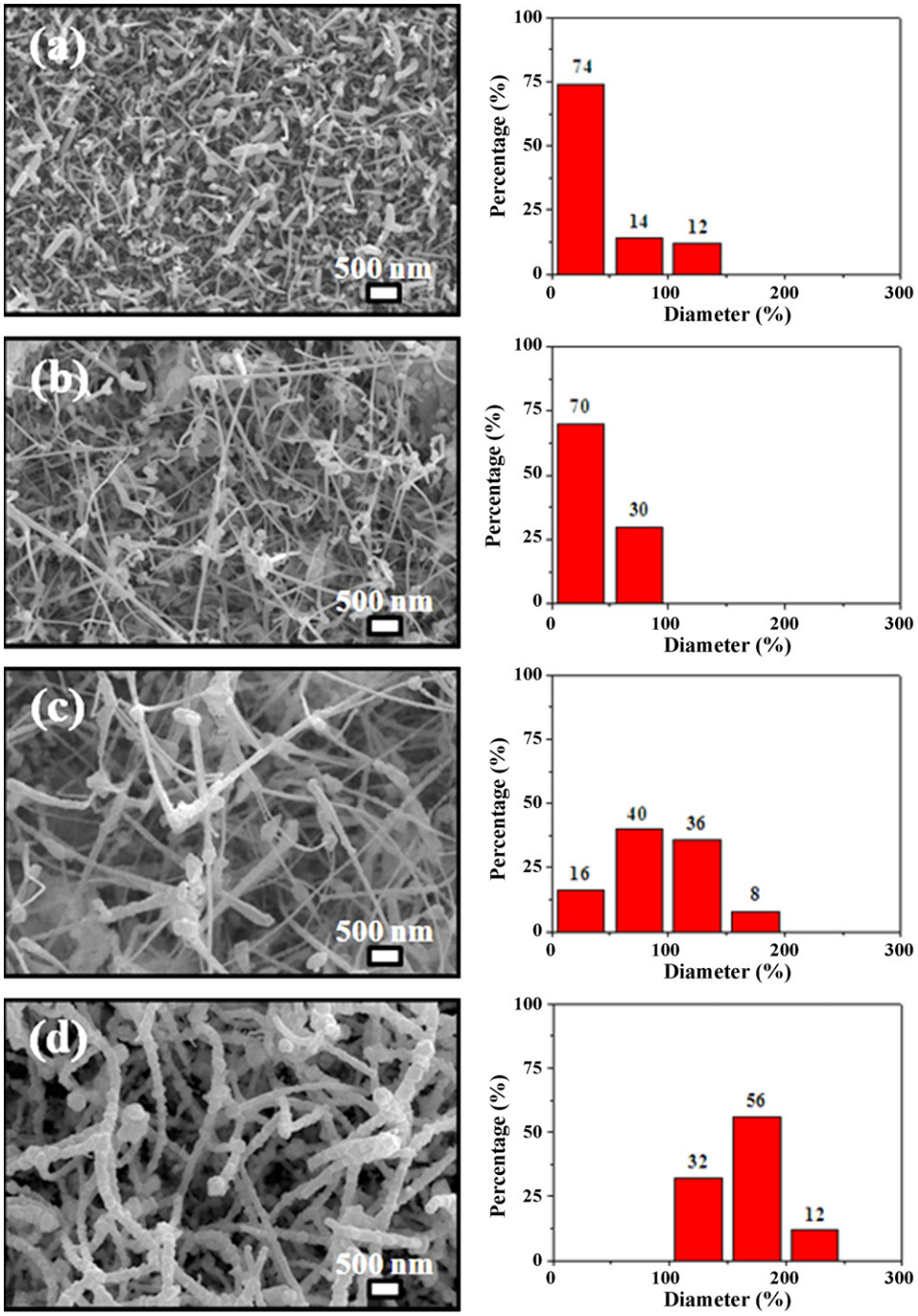

Fig. 1. SEM images and associated diameter distributions of the products grown at (a) 500, (b) 600, (c) 700, and (d) 800 °C.

product of the present study was found to vary from stem to tip region and to depend on the growth temperature.

2. Experimental

A mixture of GaN and In nanopowders were used as source materials with an 1:1 volume ratio (approximately 0.4 g in total) and were fully mixed prior to use. The synthesis of nanostructures was performed in a high-temperature quartz tube furnace [18]. The mixed powders were placed in a ceramic boat, which was put into a horizontal quartz tube. A piece of the Si plate was placed on top of the ceramic boat, acting as a substrate to collect the products. The substrate was kept at the preset temperature for 1 h under a constant flow of NH_3 (flow rate: 20 sccm) and Ar (flow rate: 100 sccm). The effects of the growth temperature was examined in the range, 500–800 °C. The as-synthesized products were examined by glancing angle (0.5°) X-ray diffraction (XRD, X'pert MPD-Philips with CuKα_1 radiation), scanning electron microscopy (SEM, Hitachi S-4200), transmission electron microscopy (TEM, Philips CM-200), and energy-dispersive X-ray (EDX) spectroscopy attached to the TEM instrument. The micro-Raman spectra were obtained using a Renishaw Raman spectromicroscope scanning from 100 cm^{-1} to 1200 cm^{-1} at room temperature in the open air. For Raman excitation, a He–Ne laser beam with a wavelength of 633 nm was used. A He–Cd laser (55 mW, wavelength at 325 nm) was employed to measure the photoluminescence (PL) of the sample.

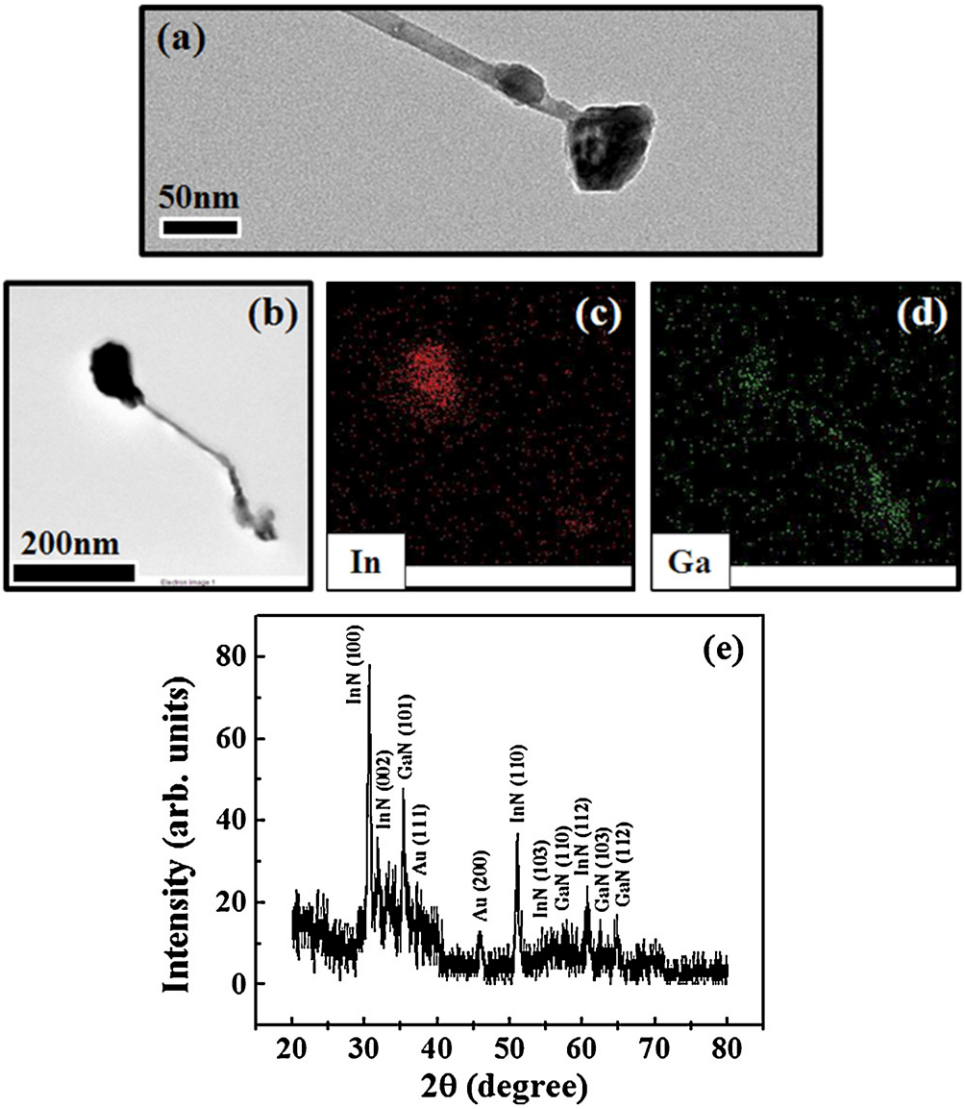

Fig. 2. (a) Low-magnification TEM image of a 600 °C-grown nanowire, (b) TEM image and corresponding elemental maps of (c) In and (d) Ga elements, and (e) XRD pattern of product synthesized at 600 °C.

3. Results and discussion

The left-hand side of Fig. 1a, b, c, and d shows typical top-view SEM images of the products grown at 500, 600, 700, and 800 °C, respectively. The diameter distributions of the products grown at 500, 600, 700, and 800 °C are shown in the right-hand side of Fig. 1a, b, c, and d, respectively. The maxima of the diameter distributions of the products grown at 500, 600, 700, and 800 °C were 0–50 nm, 0–50 nm, 50–100 nm and 150–200 nm, respectively. The mean diameter of the products grown at 500, 600, 700 and 800 °C, which was calculated from the graph of the diameter distributions, were 44, 40, 93 and 165 nm, respectively. The wire diameter tended to increase with growth temperature in the range of 600–800 °C. Although the average diameter of 500 °C-grown nanowires was slightly larger than the 600 °C-grown ones, the difference falls in the error range of the statistics.

A TEM investigation on the 600 °C-grown sample was carried out to obtain information on thinner nanowires. In addition, the 700 °C-grown product was characterized to examine the temperature effect. Fig. 2a shows a low-magnification TEM image of a 600 °C-grown product, which is a 1D nanostructure with a nanoparticle attached to its tip. Fig. 2b shows a typical TEM image, and Fig. 2c and d shows the EDX elemental maps of In and Ga. The elemental maps indicate that In and Ga elements are concentrated mainly on the tip and stem regions, respectively. Fig. 2e shows the corresponding XRD pattern. Apart from the Au-related peaks from the substrate, the diffraction peaks can be indexed to hexagonal GaN with lattice constants comparable to the values reported in the JCPDS 50-0792 card, or a hexagonal InN structure with lattice constants $a = 3.5378$ Å and $c = 5.7033$ Å (JCPDS: 50-1239).

For a detailed investigation, the lattice-resolved TEM images and SAED patterns of the tip and stem regions were examined, respectively. Fig. 3a shows a SAED pattern taken from the stem region of a nanowire. The pattern indicates a complicated structure but a closer examination reveals that it consists of ring spots corresponding to poly-crystalline hexagonal InN or poly-crystalline hexagonal GaN. The single-crystal diffraction spots were indexed as the hexagonal GaN, including (2 0 0), (3 0 3), and (1 0 3) reflections, etc. Fig. 3b shows the associated lattice resolved TEM image. The observed interplanar spacings were approximately 0.27 nm and 0.30 nm, which correspond to the separation between the neighboring (1 0 0) lattice planes of the hexagonal GaN and (1 0 0) inter-lattice distance of the hexagonal InN, respectively. According to Figs. 2 and 3, the stem part of the nanowire con-

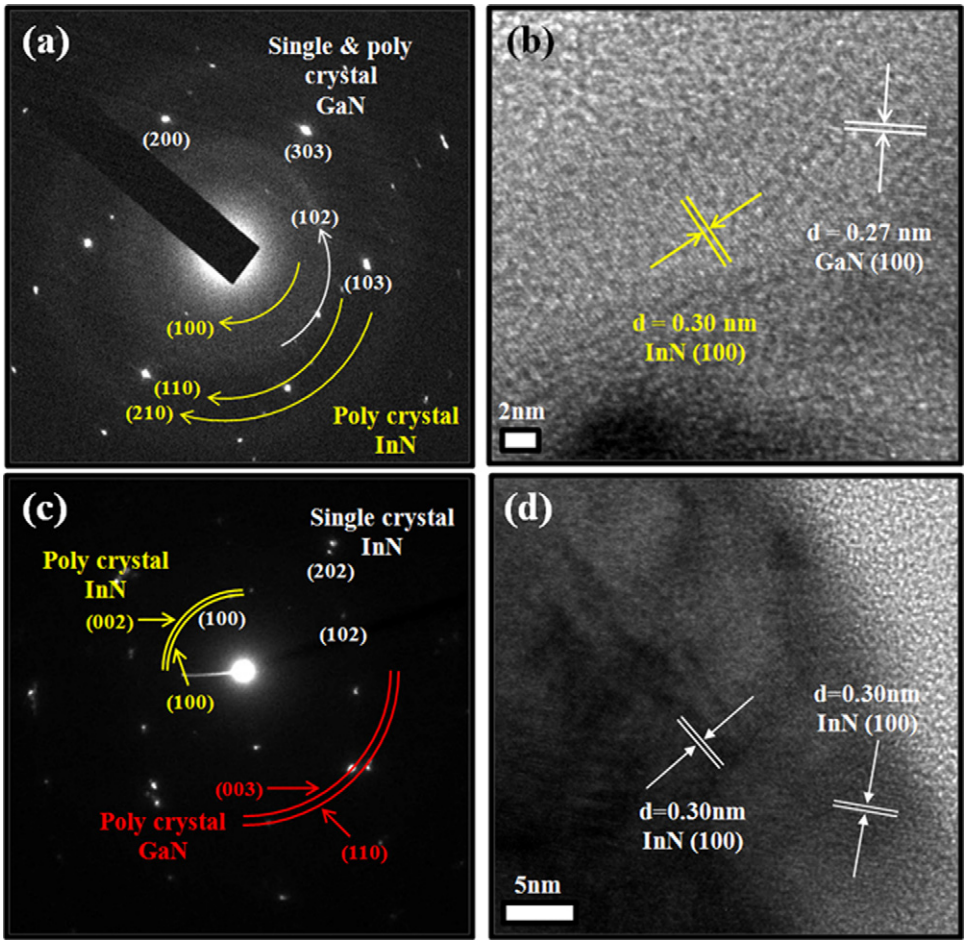

Fig. 3. (a) SAED pattern and (b) lattice-resolved TEM image taken from the stem part of the 600 °C-grown nanowire. (c) SAED pattern and (d) lattice-resolved TEM image taken from the tip part of the 600 °C-grown nanowire.

sists mainly of a hexagonal GaN phase with some additional InN phase.

On the other hand, Fig. 3c shows an SAED pattern of the tip region of a nanowire. It exhibits a spot pattern of a hexagonal InN phase, diffraction rings of hexagonal GaN phase, and InN phases. Fig. 3d shows a lattice-resolved TEM image taken from the tip of a nanowire. The measured lattice spacing of the crystalline phase was 0.30 nm, which corresponds to the (1 0 0) plane of the hexagonal InN. XRD, EDX, TEM, and SAED indicate that the tip part of the nanowire consists mainly of a hexagonal InN phase with some additional GaN phase.

Fig. 4a shows a low-magnification TEM image of a 700 °C-grown product, which consists of 1D nanostructures with a nanoparticle attached to the tip. The blackened nanoparticles are indicated by the arrowheads. Fig. 4b shows the XRD spectrum of the 700 °C-grown product. It can be seen that all the diffraction peaks can be well indexed to a hexagonal structure of InN (JCPDS: 50-1239) or a hexagonal structure of GaN (JCPDS: 50-0792). The lines observed in this diffractogram are found to coincide with (1 0 1), (1 0 2), (1 1 0), (1 0 3), and (1 1 2) peaks of hexagonal GaN and (0 0 2), (1 0 0), (1 0 1), (1 0 2), (1 1 0), (1 0 3), and (1 1 2) peaks of hexagonal InN. Fig. 4c shows a typical TEM image, whereas Fig. 4d and e shows the EDX elemental maps of In and Ga elements. Fig. 4c clearly exhibits the blackened nanoparticles, as well as the nanowires stems. Fig. 4d and e confirms that not only tip nanoparticles but also stem part contains both In and Ga elements. For In elements, however, the signal in the tip part is brighter than that in the stem part, coinciding with the quantitative investigation in Table 1. A representative EELS spectrum of a nanowire (Fig. 4f) shows characteristics edge at around 399 eV, corresponding to the K-shell ionization edge of nitrogen, respectively. The magnified result of the background subtraction clearly identifies the existence of the N–K edge, as shown in Fig. 4g.

Fig. 5a shows an SAED pattern of the stem region of a nanowire. Ring spots corresponding to the poly-crystalline hexagonal GaN can be clearly observed. Fig. 5b shows the associated lattice resolved TEM image. The fringes of the crystalline layers are separated by 0.24 nm and 0.26 nm, corresponding to the d_{101} and d_{002} of the hexagonal GaN phase. Although the SAED pattern and TEM image do not clearly exhibit an InN phase, the elemental maps in a more macroscopic view confirms the existence of In. This suggests that the stem part of the nanowire consists mainly of a hexagonal GaN phase with some additional InN phase. On the other hand, Fig. 5c shows an SAED pattern taken from the tip region of a nanowire. It indicates two sets of well-correlated diffraction spots with the diffraction rings of the hexagonal GaN and hexagonal InN phases.

Table 1
Relative atomic portions of Ga and In elements in the stem and tip parts of nanowires, based on EDX spectra.

		Ga	In	Ga + In
600	Stem	0.944	0.056	1.000
	Tip	0.006	0.994	1.000
700	Stem	0.846	0.154	1.000
	Tip	0.814	0.186	1.000

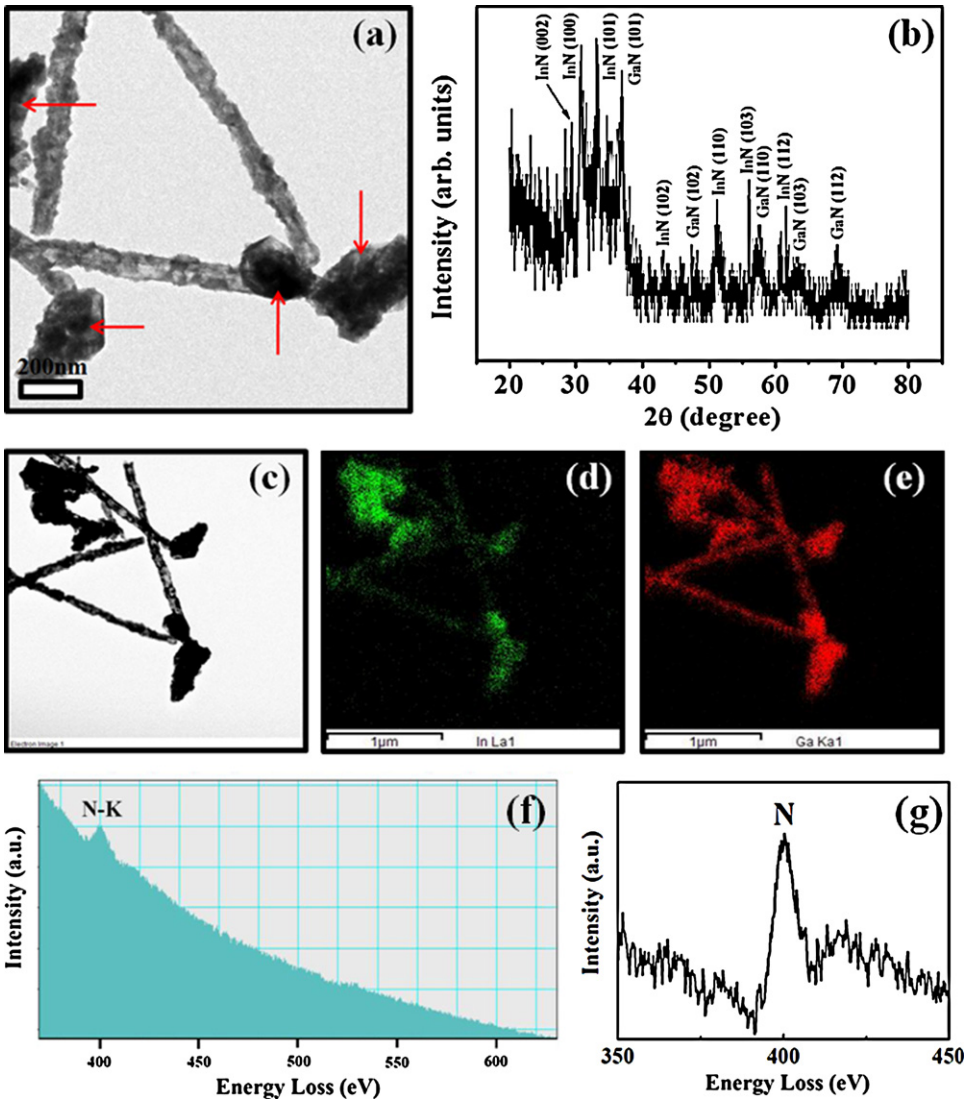

Fig. 4. (a) Low-magnification TEM image and (b) XRD pattern of 700 °C-grown nanowires. The arrowheads in (a) indicate the tip nanoparticles. (c) TEM image and corresponding elemental maps of (d) In and (e) Ga elements. (f) Representative EELS spectrum taken from a 700 °C-grown nanowire. The position of N–K edge is displayed. (g) Magnified result of the background subtraction revealing the existence of the N–K edge.

Fig. 5d shows a lattice-resolved TEM image taken from the tip part of a nanowire, revealing lattice spacings of approximately 0.20, 0.24 and 0.25 nm corresponding to the d_{102} plane of hexagonal InN, and the d_{101} and d_{002} of hexagonal GaN, respectively. XRD, EDX, TEM and SAED indicate that the tip part of the nanowire consists of hexagonal InN and GaN phases.

The growth mechanism of the 1D structures was examined based on the above observations. Both products synthesized at 600 and 700 °C consist of 1D structures with a nanoparticle attached to the tip. Accordingly, the main mechanism of the nanowires is believed to be a tip-growth VLS process. The faceted instead of spherical morphology of the tip nanoparticle might also be an indication that they were in the solid state during nanowire growth. In addition, the present mechanism can be categorized as a self-catalytic VLS process due to the absence of Au in the tip nanoparticles.

Fig. 6 shows the associated mechanisms. At 600 °C, the decomposition of GaN and In powders produces Ga and In vapors. The following reactions may explain the process: $2GaN(s) \rightarrow 2Ga(g) + N_2(g)$ [19]; and $Ga(g) + NH_3(g) \rightarrow GaN(g) + 3/2H_2(g)$ [20]. Solid In evaporates to form In vapor. The vapor may rapidly condense into the liquid Ga–In alloy clusters in air or on the surface of the substrate. Since no Au was found in the tip region, the Au element does not dissolve into In–Ga alloy droplets. Au is barely soluble in the liquid droplet for some unknown reasons. In this VLS-typed process, the vapors (e.g. Ga, In, N_2, NH_3, GaN, etc.) are incorporated onto the In–Ga liquid droplet. In particular, nitrogen atoms diffuse into the droplets, and combine with In and Ga atoms inside the droplet to form InN and GaN, respectively. Compared to conventional VLS growth, the "catalyst" (In–Ga) not only acts as the medium for transporting the component (N) from the vapor (NH_3/N_2) to the solid (InN and GaN) but also supplies the partial component (In and Ga) for the solid (InN and GaN).

On the other hand, it is likely that the Si substrate dissolves into the In–Ga liquid alloy. However, the Ga–Si and In–Si phase diagrams [21] show that In and Ga are low melting point metals with limited Si solubility and cannot form intermetallic compounds with Si. Therefore, a very low Si concentration is required in In and Ga particles to achieve saturation of the liquid alloy. Accordingly, it is believed that the incoming Si atoms quickly reach the equilibrium, resulting in the re-precipitation of solid Si. The incorporation of Si atoms is active only in the initial growth stage, in which the

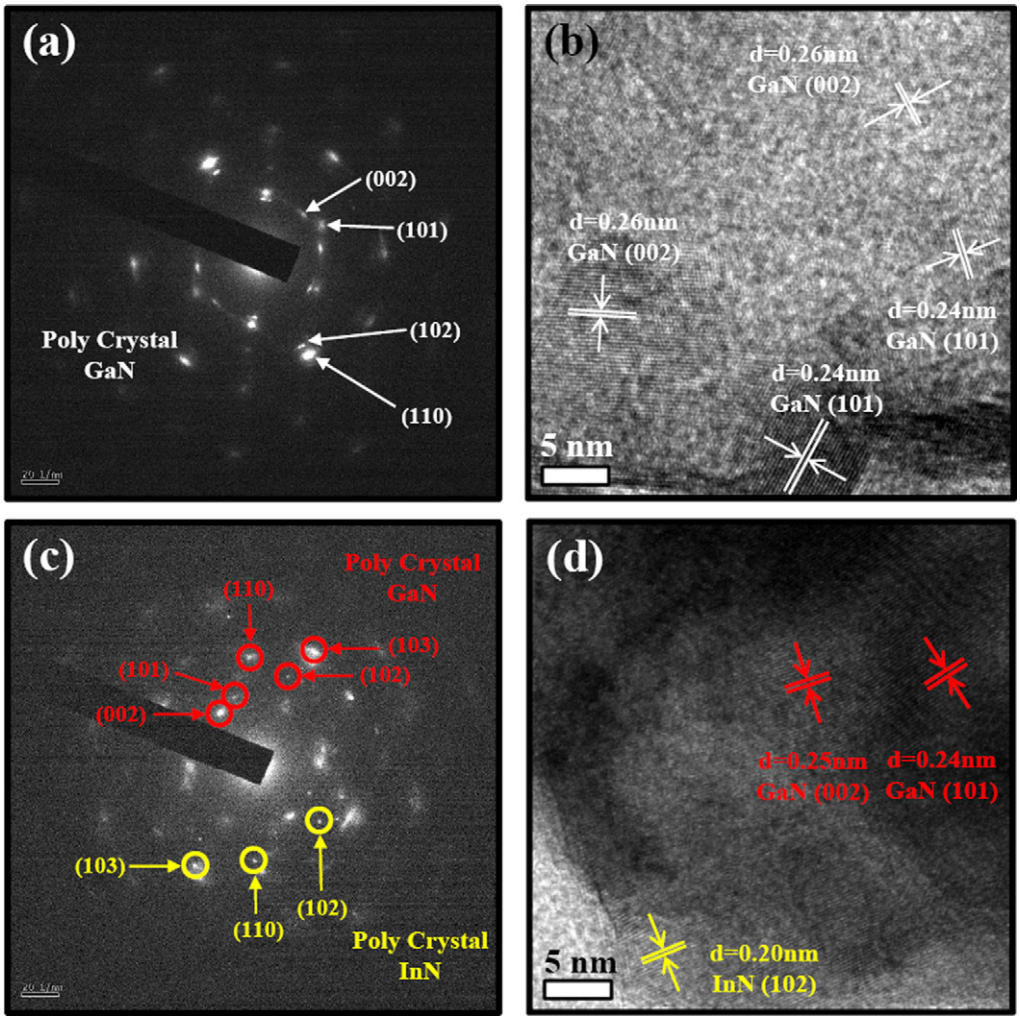

Fig. 5. (a) SAED pattern and (b) lattice-resolved TEM image taken from the stem part of the 700 °C-grown nanowires. (c) SAED pattern and (d) lattice-resolved TEM image taken from the tip part of the 700 °C-grown nanowires.

diffusion length is short. Although it is unclear in which form the Si precipitate, it is believed that a Si cluster or film-like structures precipitate on the substrates near the alloy droplets.

The vapors are transferred up to the substrate zone, and dissolve continuously into the liquid In–Ga droplets. At the early reaction stage, the dimensions of the In–Ga tip particles may be comparable to those of nanowires but the dimensions of the particles increase with the reaction time by continuously accepting the upcoming vapors. For quantitative analyses, the relative atomic portions of Ga and In elements were examined by TEM-EDX analyses (Table 1). At 600 °C, the portion of the InN phase in the tip part was far larger than that in the stem part. On the other hand, the portion of the GaN phase in the stem part is much far larger than that in the tip part. Accordingly, it is believed that the GaN structure has precipitated mainly to form nanowires. At the final stage of the growth process, the remaining In in the liquid droplets combines with nitrogen, generating an InN phase at the tips (Fig. 6). At 700 °C, for both the stem and tip regions, the portion of GaN phase is larger than that of the InN phase. However, a comparison of the tip part with the stem part suggests that the portion of the InN phase in the tip part is slightly larger than that in the stem part.

It is believed that a GaN phase can be generated by the reaction: $Ga(l) + 1/2N_2(g) \rightarrow GaN(s)$ [22]. In addition, the formation of InN can be associated with the reaction: $In(l) + 1/2N_2(g) \rightarrow InN(s)$ [23]. At 600 °C, the free energy of formation for GaN and InN is −5.85 kJ/mol and 82.23 kJ/mol, respectively. At 700 °C, the free energy of formation for GaN and InN is 6.57 kJ/mol and 93.90 kJ/mol, respectively [24]. Therefore, GaN growth is energetically more favorable than InN growth at both 600 °C and 700 °C, which can be used to explain the preferred growth of GaN-phased nanowires. Furthermore, InN usually decomposes into In and N_2 at 677–680 °C in air [21]. Accordingly, the generation and existence of InN will be suppressed at approximately 700 °C compared to the sample grown at 600 °C. From previous SEM observations (Fig. 1), the nanowire diameter tends to increase with increasing growth temperature. A high temperature provides sufficient energy to overcome the activation barrier for a variety of physical movements and chemical reactions [25,26]. It is unlikely that sidewall growth has been activated in the present VLS-typed growth because the nanowire diameter is not tapered. Instead, the higher temperature environment could have facilitated the formation of larger liquid alloy droplets on the substrate, ultimately producing nanowires with a larger diameter. Similarly, in the growth of MgO nanowires, the Au catalyst droplet size is larger at higher ambient temperatures [27].

In the VLS growth mode, the size of the nanodroplets, which serve as seeds for nanowire growth, determine the nanowire diameter [28]. In the present case, the nanowire diameter tended to increase with increasing growth temperature. We surmise that higher-temperature environment could have facilitated the formation of larger liquid alloy droplets, ultimately producing nanowires with a larger diameter. Also, previous experiments indicated that the longer growth time facilitated the growth of longer nanowires

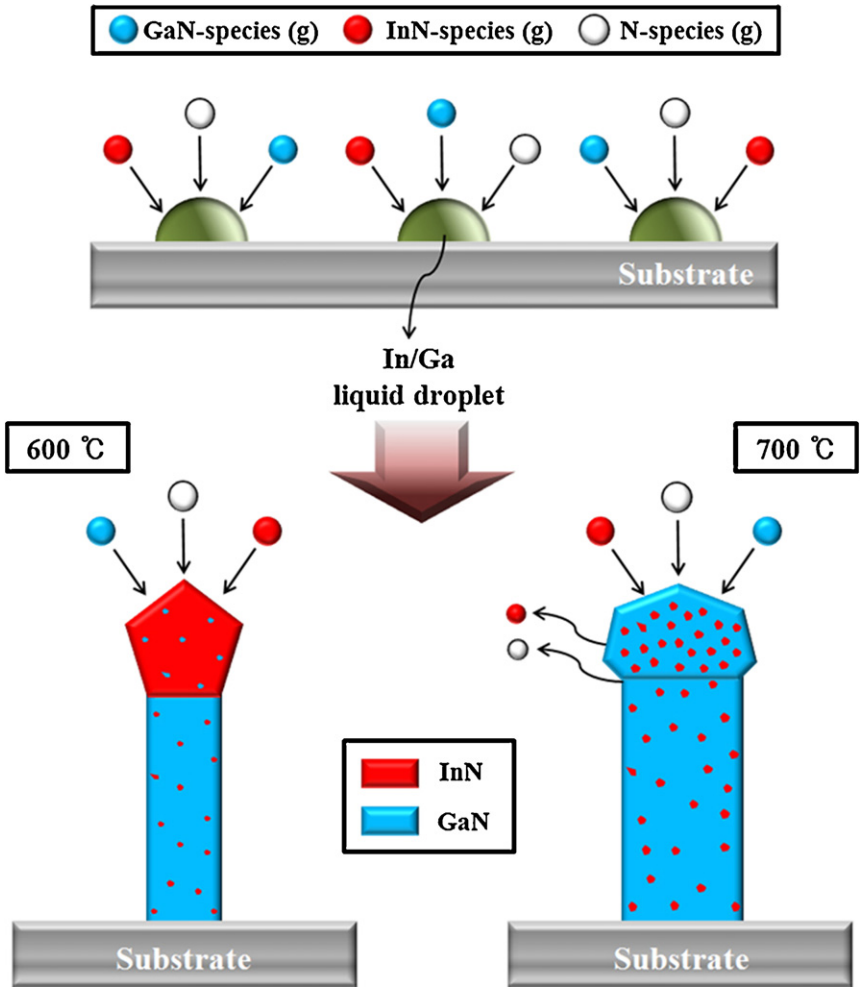

Fig. 6. Schematic illustration of the growth process at 600 °C and 700 °C. In the initial stage, a Ga–In liquid droplet is formed. The gaseous In-, Ga-, and N-related species are incorporated into the droplet, from which the composite (GaN, InN) nanowires are grown continuously. The composition is dependent on the growth temperature (600 or 700 °C) and location (stem, tip).

[29]. On the other hand, in a limited growth time, the growth rate will play a role in determining the nanowire length. For example, the supply rate of source vapor will increase with increasing the growth temperature. However, too high temperature was reported to reduce the growth rate [30] and the temperature needs to be optimized for maximum growth rate. Accordingly, we can change the characteristics of the nanowires (length, diameter, etc.) by changing the synthesis conditions.

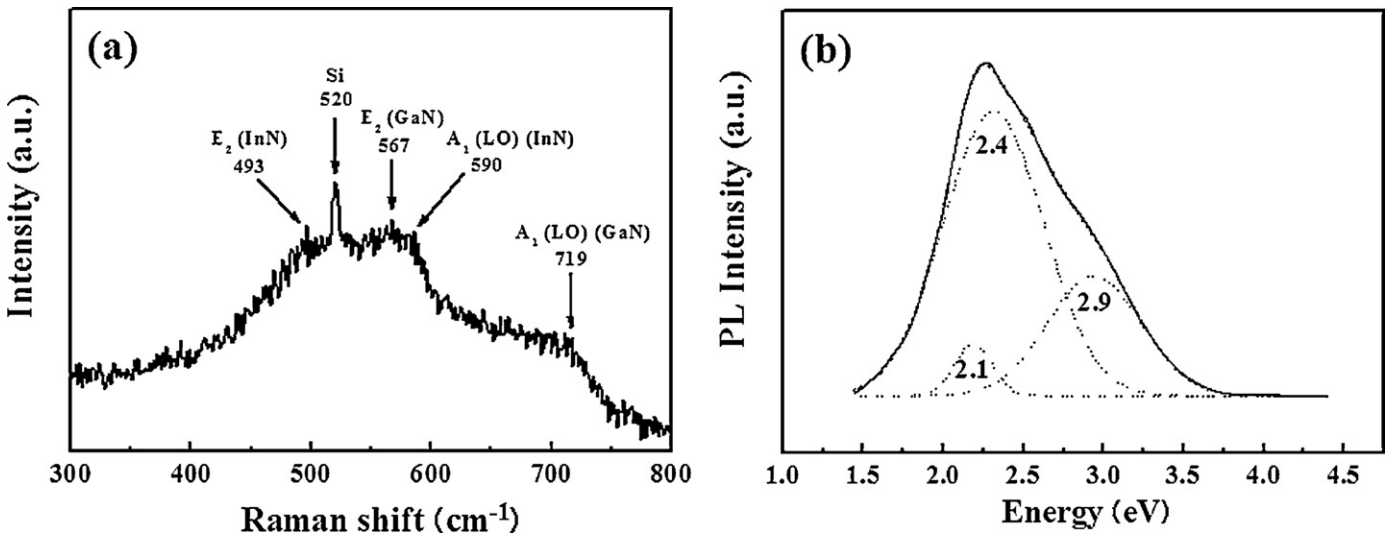

Fig. 7. (a) Raman spectrum and (b) PL spectrum of the composite nanowires.

Raman spectroscopy and PL analyses confirm the existence of the InN and GaN phases. Fig. 7a shows the room-temperature Raman spectrum of the product at 700 °C. The sharp peak at 520 cm^{-1} is identified as the TO phonon mode in the silicon (Si) crystal structure [31], presumably from Si substrates. The peak centered at 567 cm^{-1}, as the wurtzite GaN E_2 mode, is associated with the deformation potential scattering, whereas the peak at approximately 709 cm^{-1} can be assigned to the A_1(LO) mode of GaN. Besides the GaN modes, InN-related modes occur at 493 and 590 cm^{-1}, which can be assigned to the E_2 and A_1(LO) modes, respectively [32].

Fig. 7b shows the PL spectrum at room temperature. Gaussian fitting suggests that the spectrum could be divided into three Gaussian functions centered at 2.1 eV, 2.4 eV and 2.9 eV in the yellow, green and blue regions, respectively. The blue and green emissions were observed mainly in the wurtzite hexagonal GaN phase. While the blue emission in GaN was assigned to crystal defects, such as V_{Ga}-related complexes [33–35], the green emission is attributed to structural defects, including V_{Ga}, V_{Ga}–O_N complexes, etc. [33,36]. On the other hand, the 2.1-eV band is believed to have originated from the InN phase. Previously, the 2.1 eV band was observed from the PL spectrum of the InN films [37]. Both the Raman and PL spectra suggest the presence of InN and GaN phases in the products.

4. Conclusions

Novel composite nanowires were synthesized by heating a mixture of GaN and In powders. SEM shows that the nanowire diameter tends to increase with increasing growth temperature in the range of 600–800 °C. XRD, lattice-resolved TEM, SAED and EDX show that both the nanowire stem and tip parts consist of GaN and InN structures. The TEM-EDX investigation shows that the relative amounts of GaN and InN phases are dependent on the growth temperature and location in the nanowire (i.e. stem or tip). At the tip, the formation of an InN phase tends to be favorable at 600 °C, whereas the InN phase reduces at 700 °C. The possible growth mechanism of the composite nanowires was discussed including the reason for the compositional changes. The existence of a composite (GaN, InN) particle at the tip suggests that the growth mechanism is dominated by a self-catalytic VLS process. Raman and PL spectra suggest the presence of an InN and GaN phase in the composite nanowires. By choosing the appropriate source materials, this method can be extended and exploited to produce nanowire-nanoparticle composites of other materials.

Acknowledgement

This research was supported by National Nuclear R&D Program through the National Research Foundation of Korea (NRF) funded by the Ministry of Education, Science and Technology (2010-0018699).

References

[1] M.T. Bjork, B.J. Ohlsson, C. Thelander, A.I. Persson, K. Deppert, L.R. Wallenberg, L. Samuelson, Nanowire resonant tunneling diodes, Appl. Phys. Lett. 81 (2002) 4458–4460.
[2] J. Wensorra, K.M. Indlekofer, M.I. Lepsa, A. Föster, H. Lüth, Resonant tunneling in nanocolumns improved by quantum collimation, Nano Lett. 5 (2005) 2470–2475.
[3] C. Thelander, T. Martensson, M.T. Bjork, B.J. Ohlsson, M.W. Larsson, L.R. Wallenberg, L. Samuelson, Single-electron transistors in heterostructure nanowires, Appl. Phys. Lett. 83 (2003) 2052–2054.
[4] M.T. Borgström, V. Zwiller, E. Müller, A. Imamoglu, Optically bright quantum dots in single nanowires, Nano Lett. 5 (2005) 1439–1443.
[5] H. Petterson, J. Trägardh, A.I. Persson, L. Landin, D. Hessman, L. Samuelson, Infrared photodetectors in heterostructure nanowires, Nano Lett. 6 (2006) 229–232.
[6] J.L. Johnson, Y. Cjoi, A. Ural, W. Lim, J.S. Wright, B.P. Gila, F. Ren, S.J. Pearton, Growth and characterization of GaN nanowires for hydrogen sensors, J. Electron. Mater. 38 (2009) 490–494.
[7] H. Morkoc, S.N.S.N. Mohammad, High-luminosity blue and blue-green gallium nitride light-emitting diodes, Science 267 (1995) 51–55.
[8] F.A. Ponce, D.P. Bour, Nitride-based semiconductors for blue and green light-emitting devices, Nature 386 (1997) 351–359.
[9] N. Mohammad, H. Morkoc, Progress and prospects of group-III nitride semiconductors, Prog. Quantum Electron. 20 (1996) 361–525.
[10] I. Vurgaftman, J.R. Meyer, Band parameters for nitrogen-containing semiconductors, J. Appl. Phys. 94 (2003) 3675–3696.
[11] Z. Qian, S. Hou, J. Zhang, R. Li, Z. Shen, X. Zhao, Z. Xue, Stability and electronic structure of single-walled InN nanotubes, Physica E 30 (2005) 81–85.
[12] A.G. Bhuiyan, A. Hashimoto, A. Yamamoto, Indium nitride (InN): a review on growth, characterization, and properties, J. Appl. Phys. 94 (2003) 2779–2808.
[13] A. Yamamoto, M. Tsujino, M. Ohkubo, A. Hashimoto, Metalorganic chemical vapor deposition growth of InN for InN/Si tandem solar cell, Sol. Energy Mater. Sol. Cells 35 (1994) 53–60.
[14] Z.G. Qian, W.Z. Shen, H. Ogawa, Q.X. Guo, Infrared reflection characteristics in InN thin films grown by magnetron sputtering for the application of plasma filters, J. Appl. Phys. 92 (2002) 3683–3687.
[15] W.-H. Chang, W.-C. Ke, S.-H. Yu, L. Lee, C.-Y. Chen, W.-C. Tsai, H. Lin, W.-C. Chou, M.-C. Lee, W.-K. Chen, Effects of growth temperature on InN/GaN nanodots grown by metal organic chemical vapor deposition, J. Appl. Phys. 103 (2008) 104306.
[16] N.C. Chen, P.H. Chang, Y.N. Wang, H.C. Peng, W.C. Lien, C.F. Shih, C.-A. Chang, G.M. Wu, Schottky behavior at InN–GaN interface, Appl. Phys. Lett. 87 (2005) 212111.
[17] Y.H. Kim, H.J. Park, K. Kim, C.S. Kim, W.S. Yun, J.W. Lee, M.D. Kim, Strain distribution and interface modulation of highly lattice-mismatched InN/GaN heterostructure nanowires, Appl. Phys. Lett. 95 (2009) 033112.
[18] J.C. Yang, H.G. Na, M.A. Kebede, H.S. Kim, H.W. Kim, GaN-cored heteronanowires sheathed with Pt shells: preparation and annealing studies, J. Cryst. Growth 312 (2010) 1199–1204.
[19] J.-S. Lee, K. Park, S. Nahm, S.-W. Kim, S. Kim, Ga_2O_3 nanomaterials synthesized from ball-milled GaN powders, J. Cryst. Growth 244 (2002) 287–295.
[20] J. Li, C. Lu, B. Maynor, S. Huang, J. Liu, Controlled growth of long GaN nanowires from catalyst patterns fabricated by "Dip-Pen" nanolithographic techniques, Chem. Mater. 16 (2004) 1633–1636.
[21] T.B. Massalski, H. Okamoto, P.R. Subramanian, L. Kacprozak, Binary Alloy Phase Diagrams, ASM Int., Materials Park, OH, 1992.
[22] K.T. Jacob, S. Singh, Y. Waseda, Refinement of thermodynamic data on GaN, J. Mater. Res. 22 (2007) 3475–3483.
[23] J. Leitner, P. Marsik, D. Sedmidubsky, K. Ruzicka, High temperature enthalpy, heat capacity and other thermodynamic functions of solid InN, J. Phys. Chem. Solids 65 (2004) 1127–1131.
[24] I. Barin, Thermochemical Data of Pure Substances, VCH, New York, 1989.
[25] P. Paiano, P. Prete, Size and shape control of GaAs nanowires grown by metalorganic vapor phase epitaxy using tertiarybutylarsine, J. Appl. Phys. 100 (2006) 094305.
[26] H. Srivastava, P. Tiwari, A.K. Srivastava, R.V. Nandedkar, Growth and characterization of α-Fe_2O_3 nanowires, J. Appl. Phys. 102 (2007) 054303.
[27] K. Nagashima, T. Yanagida, H.H. Tanaka, T. Kawai, Control of magnesium oxide nanowire morphologies by ambient temperature, Appl. Phys. Lett. 90 (2007) 233103.
[28] V. Schmidt, U. Gösele, How nanowires grow, Science 316 (2007) 698–699.
[29] S. Kodambaka, J. Tersoff, M.C. Reuter, F.M. Ross, Germanium nanowire growth below the eutectic temperature, Science 316 (2007) 729–732.
[30] K. Nagashima, T. Yanagida, H. Tanaka, T. Kawai, Control of magnesium oxide nanowire morphologies by ambient temperature, Appl. Phys. Lett. 90 (2007) 233103.
[31] M. Hirasawa, T. Orii, T. Seto, Size-dependent crystallization of Si nanoparticles, Appl. Phys. Lett. 88 (2006) 093119.
[32] H.-J. Kwon, Y.-H. Lee, O. Miki, H. Yamano, A. Yoshida, Raman spectra of indium nitride thin films grown by microwave-excited metalorganic vapor phase epitaxy on (0001) sapphire substrates, Appl. Phys. Lett. 69 (1996) 937–939.
[33] M.A. Reshchikov, H. Morkoc, Luminescence properties of defects in GaN, J. Appl. Phys. 97 (2005) 061301.
[34] M.A. Reshchikov, R.Y. Korotkov, Analysis of the temperature and excitation intensity dependencies of photoluminescence in undoped GaN films, Phys. Rev. B 64 (2001) 115205.
[35] H.C. Yang, T.Y. Lin, Y.F. Chen, Nature of the 2.8-eV photoluminescence band in Si-doped GaN, Phys. Rev. B 62 (2000) 12593–12596.
[36] M.A. Reshchikov, H. Morkoc, S.S. Park, K.Y. Lee, Yellow and green luminescence in a freestanding GaN template, Appl. Phys. Lett. 78 (2001) 3041–3043.
[37] T. Yodo, H. Yona, H. Ando, D. Nosei, Y. Harada, Strong band edge luminescence from InN films grown on Si substrates by electron cyclotron resonance-assisted molecular beam epitaxy, Appl. Phys. Lett. 80 (2002) 968–970.